Nde1 promotes diverse dynein functions through differential interactions and exhibits an isoform-specific proteasome association

Julie K. Monda and Iain M. Cheeseman*
Whitehead Institute for Biomedical Research, Cambridge, MA 02142; Department of Biology, Massachusetts Institute of Technology, Cambridge, MA 02142

ABSTRACT **Nde1 is a key regulator of cytoplasmic dynein, binding directly to both dynein itself and the dynein adaptor, Lis1. Nde1 and Lis1 are thought to function together to promote dynein function, yet mutations in each result in distinct neurodevelopment phenotypes. To reconcile these phenotypic differences, we sought to dissect the contribution of Nde1 to dynein regulation and explore the cellular functions of Nde1. Here we show that an Nde1–Lis1 interaction is required for spindle pole focusing and Golgi organization but is largely dispensable for centrosome placement, despite Lis1 itself being required. Thus, diverse functions of dynein rely on distinct Nde1- and Lis1-mediated regulatory mechanisms. Additionally, we discovered a robust, isoform-specific interaction between human Nde1 and the 26S proteasome and identify precise mutations in Nde1 that disrupt the proteasome interaction. Together, our work suggests that Nde1 makes unique contributions to human neurodevelopment through its regulation of both dynein and proteasome function.**

Monitoring Editor
Keith G. Kozminski
University of Virginia

Received: Jul 5, 2018
Accepted: Jul 13, 2018

INTRODUCTION

Cytoplasmic dynein is the primary cellular minus-end-directed microtubule motor and is therefore a key contributor to diverse cellular processes (Kardon and Vale, 2009). Spatial and temporal control of dynein function relies on its regulation by the noncatalytic subunits of the dynein complex, as well as adaptor proteins such as dynactin, Lis1, and Nde1 (Kardon and Vale, 2009). Nde1 directly interacts with multiple subunits of the dynein complex, as well as Lis1 (Bradshaw and Hayashi, 2017), and is thought to help tether Lis1 to the dynein complex to facilitate dynein function (McKenney *et al.*, 2010; Wang and Zheng, 2011; Huang *et al.*, 2012). However, the precise mechanisms underlying Nde1-mediated regulation of diverse dynein functions remain unclear.

In humans, mutations in Nde1 result in severe reductions in brain size (microcephaly) and neuronal lamination defects such as lissencephaly (Alkuraya *et al.*, 2011; Bakircioglu *et al.*, 2011; Guven *et al.*, 2012; Paciorkowski *et al.*, 2013; Tan *et al.*, 2017). In contrast, mutations in Lis1 cause lissencephalic, but not microcephalic, phenotypes (Dobyns and Das, 2009). Thus, neurodevelopment likely depends on the coordinated activities of Nde1 and Lis1 in dynein regulation, as well as additional Lis1-independent functions of Nde1. Humans ubiquitously express two alternative splice isoforms of Nde1 throughout the brain that differ in their last exon: Nde1_SSSC and Nde1_KMLL (named for their four C-terminal residues; see Bradshaw *et al.* (2009). Nde1_KMLL is the human homologue of the canonical mouse Nde1 isoform. In contrast, Nde1_SSSC is generally considered the canonical human isoform but is comparatively recently evolved (Bradshaw *et al.*, 2009; Mosca *et al.*, 2017), having annotated homologues only in a few species of primates and dog. Interestingly, knockout of Nde1 in mice does result in microcephaly, but the severity does not recapitulate the effect seen in human patients (Bakircioglu *et al.*, 2011), suggesting the possibility of human-specific contributions from Nde1 to brain development.

Here we use cell biological and biochemical approaches to probe the cellular functions of human Nde1. First, we used a CRISPR/Cas9-based replacement assay to robustly define the contribution of Nde1 to dynein regulation. Our analyses reveal that the direct interactions between Nde1 and Lis1 or dynein differentially contribute to diverse dynein activities. Thus, dynein regulation is achieved not simply by the presence of particular adaptors but

This article was published online ahead of print in MBoC in Press (http://www.molbiolcell.org/cgi/doi/10.1091/mbc.E18-07-0418) on July 19, 2018.
*Address correspondence to: Iain M. Cheeseman (icheese@wi.mit.edu).
Abbreviations used: DHC, dynein heavy chain; DIC, dynein intermediate chain.

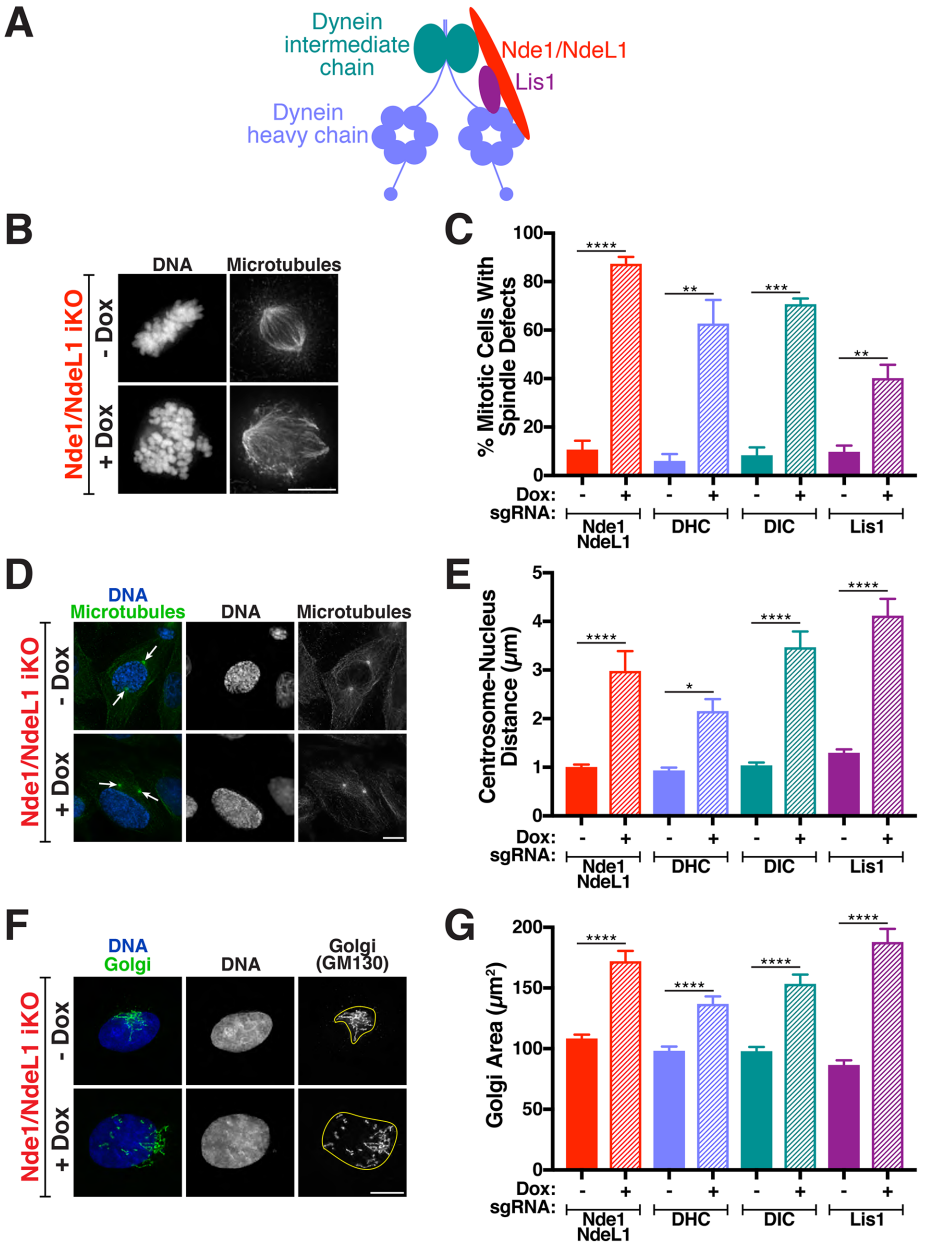

FIGURE 1: Nde1 and NdeL1 regulate diverse dynein-dependent cellular processes. (A) Cartoon of Nde1/NdeL1 illustrating interactions with Lis1 and the dynein heavy and intermediate chains. (B) Immunofluorescence images of DNA (Hoechst) and microtubules (DM1A) for the indicated conditions, illustrating the spindle pole focusing defects after elimination of Nde1 and NdeL1. Scale bar, 10 μm. (C) Quantification of the spindle pole focusing defects for the indicated conditions. The data represent the replicate mean + SD. Each replicate included 100 cells. Three replicates were analyzed for all conditions, except Lis1 –/+ Dox where five replicates were analyzed. Statistical significance was determined by two-tailed unpaired *t* tests. ****$p \leq 0.0001$; ***$p \leq 0.001$; **$p \leq 0.01$. (D) Immunofluorescence images of DNA (Hoechst, blue) and microtubules (DM1A, green) for the indicated conditions illustrating the prophase centrosome placement defects after elimination of Nde1 and NdeL1. Arrows indicate the centrosomes, inferred by the foci of microtubule nucleation. Scale bar, 10 μm. (E) Quantification of centrosome–nucleus distances for the indicated conditions. The data represent the mean distance for all measured centrosomes + SEM. Data were combined from three replicates for each condition. Across all replicates, the following numbers of centrosomes were analyzed: Nde1/NdeL1 iKO –/+ Dox – 150; DHC iKO –/+ Dox – 150; DIC iKO –/+ Dox – 140; Lis1 iKO –/+ Dox – 138. Statistical significance was determined by two-tailed Mann–Whitney tests. ****$p \leq 0.0001$; *$p \leq 0.05$. (F) Immunofluorescence images of DNA (Hoechst, blue) and Golgi (GM130, green) for the indicated conditions illustrating the Golgi organization defects after elimination of Nde1 and NdeL1. The yellow outline in the Golgi (GM130) panel indicates the region occupied by the Golgi. Scale bar, 10 μm. (G) Quantification of the area occupied by the Golgi, measured in Metamorph, for the indicated conditions. The data represent the mean area for all measured Golgi + SEM. Data were combined from two to three replicates for each condition. Across all replicates, the following numbers of cells were analyzed: Nde1/NdeL1 iKO – Dox, 351; Nde1/NdeL1 iKO + Dox, 236; DHC iKO – Dox, 257; DHC iKO + Dox, 201; DIC iKO – Dox, 296; DIC iKO + Dox, 197; Lis1 iKO – Dox, 222; Lis1 iKO + Dox, 210. Statistical significance was determined by two-tailed Mann–Whitney tests. ****$p \leq 0.0001$.

instead by the specific intermolecular interactions utilized within the dynein-adaptor complex. Second, we used mass spectrometry to broadly explore Nde1 function and uncovered an interaction between the canonical human Nde1 isoform and the 26S proteasome. Together, the results define an additional role for Nde1 in dynein regulation beyond its role in recruiting Lis1 and identify a recently evolved interaction between Nde1 and the proteasome in human cells.

RESULTS

Nde1 promotes diverse functions of cytoplasmic dynein

Nde1 binds directly to both dynein and Lis1 (Figure 1A), and prior work suggests that Nde1 contributes to dynein regulation by helping recruit Lis1 to dynein (Wang and Zheng, 2011; Huang *et al.*, 2012). To test the contribution of the Nde1-Lis1 interaction to diverse cellular functions of dynein, we utilized an inducible CRISPR/Cas9 system in human cells. Because of the redundant roles of Nde1 and its paralogue, NdeL1, in dynein regulation in cell culture (Lam *et al.*, 2010; Bolhy *et al.*, 2011; Raaijmakers *et al.*, 2013; McKinley and Cheeseman, 2017), we simultaneously expressed single guide RNAs (sgRNAs) targeting Nde1 and NdeL1 in cells containing Cas9 under the control of a doxycycline-inducible promoter (McKinley and Cheeseman, 2017). Cas9 induction in these cells resulted in multiple cellular defects. First, we observed an accumulation of cells in mitosis due to a failure to generate a bipolar mitotic spindle. Instead, the microtubules of the spindle were frequently unfocused (Figure 1, B and C) (Raaijmakers *et al.*, 2013; McKinley and Cheeseman, 2017). Despite these spindle defects, the vast majority of prophase cells showed two clear foci of centrosome-derived microtubule nucleation (unpublished data) indicating that the resulting unfocused spindles are not due to

alterations in prophase centrosome numbers. However, the prophase centrosomes were often mispositioned. Instead of being juxtanuclear, we observed an increased incidence of centrosomes that were detached from the nuclear envelope during prophase (Figure 1, D and E) (Bolhy *et al.*, 2011; Raaijmakers *et al.*, 2013). Finally, we also observed defects in the organization of the Golgi apparatus during interphase. In control cells, the Golgi are positioned adjacent to the nucleus and are relatively compact (Figure 1, F and G). After knockout of Nde1 and NdeL1, the Golgi are frequently fragmented and dispersed throughout the cell (Figure 1, F and G) (Lam *et al.*, 2010).

To compare these phenotypes to the effects of dynein depletion, we also analyzed inducible knockout cells expressing an sgRNA targeting either dynein heavy chain (DHC) or dynein intermediate chain (DIC). DHC contains the motor domain of the dynein complex, and DIC is an additional dynein subunit that binds directly to Nde1 (Figure 1A) (Wang and Zheng, 2011). Cas9 expression in these DHC or DIC inducible knockout cells recapitulated all three phenotypes observed after knockout of Nde1 and NdeL1 (Figure 1, C, E, and G, and Supplemental Figure S1), consistent with Nde1/NdeL1 contributing to dynein function in mitotic spindle organization, prophase centrosome placement, and Golgi organization.

Finally, we tested the requirement of Lis1 for dynein function using our inducible CRISPR/Cas9 system. As we observed following loss of Nde1/NdeL1, we found that eliminating Lis1 also caused defects in spindle pole focusing, centrosome placement, and Golgi organization (Figure 1, C, E, and G, and Supplemental Figure S1). Together, these results define a requirement for Nde1/NdeL1, the cytoplasmic dynein complex, and Lis1 in bipolar spindle assembly, centrosome positioning during prophase, and interphase Golgi organization in human cells.

Distinct dynein activities require different Nde1 interactions

To define the contribution of Nde1 to dynein regulation, we expressed wild-type or mutant versions of Nde1 that disrupt specific interactions (Figure 2A and Supplemental Figure S2) (Derewenda *et al.*, 2007; Wang and Zheng, 2011; Wang *et al.*, 2013) in the background of our Nde1/NdeL1 inducible knockout cells. As expected given the functional redundancy of Nde1 and NdeL1 in dynein regulation, expression of wild-type Nde1 alone was able to fully rescue the spindle pole focusing, centrosome placement, and Golgi organization defects of the Nde1/NdeL1 double knockout (Figure 2, B–G).

Next, we analyzed the contribution of the Nde1–DIC and Nde1–Lis1 interactions to spindle pole focusing. Although DIC is required for spindle pole focusing (Figure 1C and Supplemental Figure S1A), the DIC binding mutant, Nde1^{E47A}, largely restored the spindle defects of the Nde1/NdeL1 double knockout (Figure 2, B and C). In contrast, eliminating the Nde1–Lis1 interaction by expressing Nde1$^{E118A\ R129A}$ resulted in severe spindle pole focusing defects (Figure 2, B and C). Thus, bipolar spindle assembly critically depends on an Nde1-Lis1 interaction, but not an Nde1-DIC interaction, despite the important role for DIC itself in this process.

To determine whether binding of Nde1 to Lis1 is a general requirement for dynein function, we next tested the mechanism by which Nde1 contributes to the positioning of the centrosomes during prophase. Although the Nde1–DIC interaction was not required for bipolar spindle assembly (Figure 2, B and C), disrupting the Nde1–DIC interaction through expression of the Nde1^{E47A} mutant did not rescue the centrosome placement defects (Figure 2, D and E). These data not only demonstrate a key role for an Nde1-DIC interaction in centrosome placement but also indicate that mispositioned centrosomes at the onset of mitosis can still generate a bipolar spindle (see also Bolhy *et al.*, 2011). Strikingly, the Nde1$^{E118A\ R129A}$ mutant, which prevents the Lis1 interaction, largely restored prophase centrosome placement (Figure 2, D and E), although depletion of Lis1 itself did result in detached centrosomes (Figure 1E and Supplemental Figure S1B). Thus, proper centrosome placement requires Lis1 protein and an Nde1–DIC interaction but not a direct Nde1–Lis1 interaction.

Finally, as our analyses indicate that dynein function in mitotic spindle pole focusing and prophase centrosome positioning require distinct functional interactions, we sought to define the regulatory mechanisms required to organize the Golgi apparatus during interphase. Similarly to the results of our spindle pole focusing analysis, expression of the DIC binding mutant, Nde1^{E47A}, largely restored Golgi organization (Figure 2, F and G), despite DIC itself being required (Figure 1G and Supplemental Figure S1C). However, the Golgi was fragmented in cells expressing the Lis1 binding mutant, Nde1$^{E118A\ R129A}$ (Figure 2, F and G), suggesting that the Nde1–Lis1 interaction is required for the proper function of dynein in the organization of the Golgi apparatus, as well as bipolar spindle assembly.

Together, these data demonstrate that Nde1 utilizes multiple mechanisms to regulate dynein function. Although an Nde1–Lis1 interaction is critically required for bipolar spindle assembly and Golgi organization, it is not required to position the centrosomes at the nuclear envelope during prophase. Thus, Nde1 is not solely acting as a recruitment factor for Lis1. Furthermore, these findings highlight that even when controlled by the same molecular players, different cellular dynein functions rely on distinct regulatory mechanisms.

Nde1_SSSC immunoprecipitates the 26S proteasome

Mutations in Nde1 and Lis1 in human patients result in distinct phenotypic consequences, yet our analyses of their cellular contributions above did not reveal Nde1-specific phenotypes. Because Nde1 results in even more severe brain development phenotypes in humans than mice, we speculated that the recently evolved human isoform, Nde1_SSSC, may exhibit novel functionality. Numerous binding partners have been reported for Nde1 (Bradshaw *et al.*, 2013), but the majority of this work has not utilized human Nde1. We therefore sought to broadly explore cellular functions of Nde1_SSSC using immunoprecipitation-mass spectrometry to probe for novel interactions. Because Nde1 has known roles during both interphase and mitosis, we performed affinity purifications from asynchronous and mitotic populations of HeLa cells stably expressing green fluorescent protein (GFP)-Nde1_SSSC. We identified established interacting partners of Nde1 including NdeL1, dynein, and CENP-F (Figure 3A and Supplemental Table S1) (Bradshaw *et al.*, 2013). Strikingly, in both the asynchronous and mitotic immunoprecipitations, we also identified substantial numbers of peptides from most of the subunits of the 26S proteasome (Figure 3A and Supplemental Table S1). In contrast, when we used identical antibody and purification conditions to isolate GFP-Nde1_KMLL or GFP-NdeL1 from HeLa cells, we identified only background amounts of proteasome subunits (two peptides total; Figure 3A and Supplemental Table S1), suggesting that the proteasome interaction is specific to Nde1_SSSC. To test whether the Nde1_SSSC-proteasome interaction also occurs in other cell types, we next immunoprecipitated GFP-Nde1_SSSC from U2OS cells. Again, we identified hundreds of proteasomal peptides (Figure 3B and Supplemental Table S1). However, immunoprecipitation of Nde1_KMLL isolated only eight proteasomal peptides (Figure 3B and Supplemental Table S1). Additionally, we found that the Nde1–proteasome interaction is remarkably stable, as we still detected substantial proteasomal peptides after washing the Nde1-bound

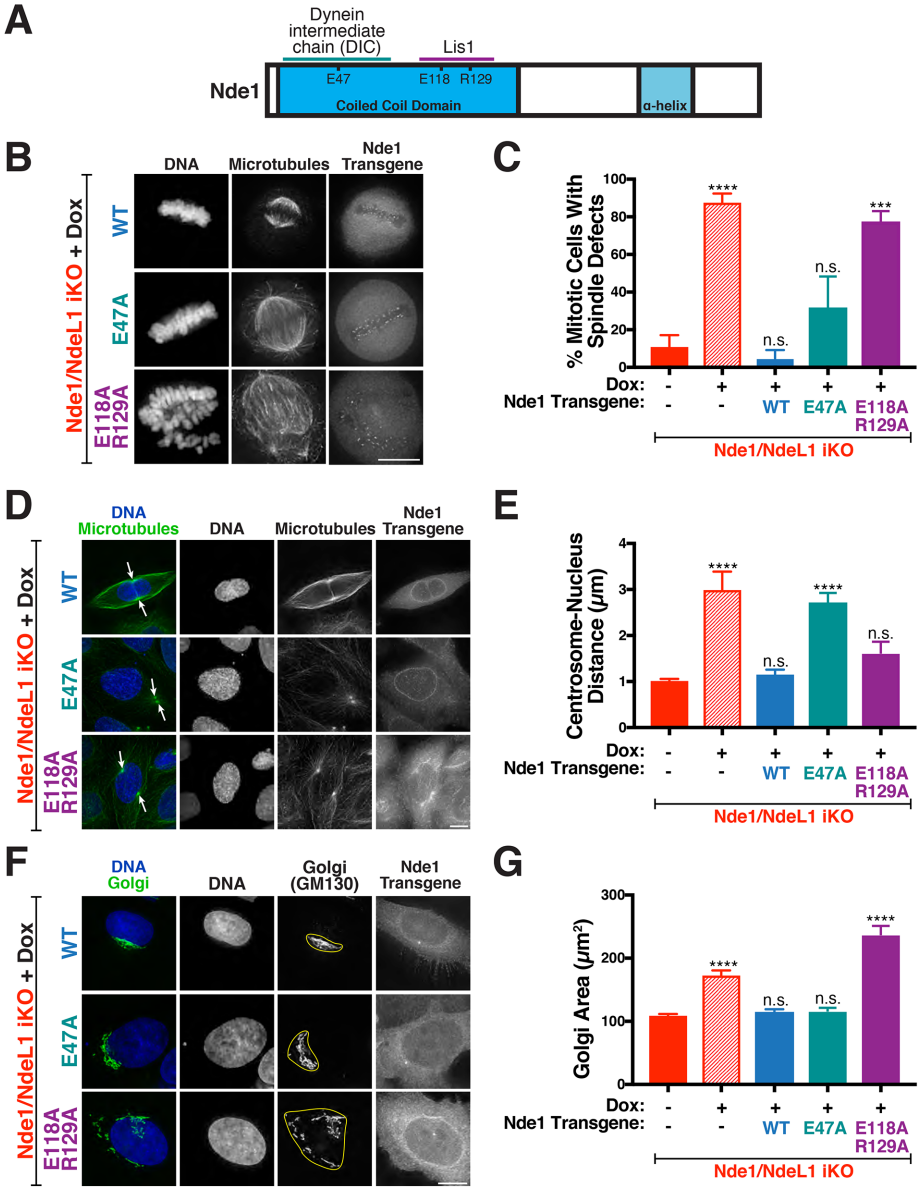

FIGURE 2: Distinct Nde1 interactions are required for different functions of dynein. (A) Schematic of Nde1 depicting structural features, as well as mapped binding sites and key interaction residues for the indicated proteins (Yan *et al.*, 2003; Tarricone *et al.*, 2004; Bradshaw *et al.*, 2009; Wang and Zheng, 2011; Zylkiewicz *et al.*, 2011; Soares *et al.*, 2012). The residues shown indicate the corresponding Nde1 residue number for mutations defined in NdeL1. (B) Immunofluorescence images of DNA (Hoechst), microtubules (DM1A), and wild-type (WT) or mutant GFP-Nde1 4 d after Cas9 induction with doxycycline. Scale bar, 10 μm. (C) Quantification of the spindle pole focusing defects for the indicated conditions. The data for Nde1/NdeL1 iKO –/+ Dox are duplicated from Figure 1C. The data represent the mean of three replicates + SD. Each replicate included ≥ 15 cells. Across all replicates, the following numbers of cells were analyzed: WT, 58; E47A, 56; E118A R129A, 99. Statistical significance relative to control cells (Nde1/NdeL1 iKO – Dox) was determined by two-tailed unpaired *t* tests. ****$p \leq 0.0001$; ***$p \leq 0.001$; n.s., $p > 0.05$. (D) Immunofluorescence images of DNA (Hoechst, blue), microtubules (DM1A, green), and WT or mutant GFP-Nde1 for the indicated conditions. Arrows indicate the centrosomes, inferred by the foci of microtubule nucleation. Scale bar, 10 μm. (E) Quantification of the centrosome-nucleus distances for the indicated conditions. The data for Nde1/NdeL1 iKO –/+ Dox are duplicated from Figure 1E. The data represent the mean distance for all measured centrosomes + SEM. Data were combined from three or four replicates for each condition. Across all replicates, the following numbers of centrosomes were analyzed: WT, 50; E47A, 120; E118A R129A, 116. Statistical significance relative to control cells (Nde1/NdeL1 iKO – Dox) was determined by two-tailed Mann-Whitney tests. ****$p \leq 0.0001$; n.s., $p > 0.05$. (F) Immunofluorescence images of DNA (Hoechst, blue), Golgi (GM130, green), and WT or mutant GFP-Nde1 for the indicated conditions. The yellow outline in the Golgi (GM130) panel indicates the region occupied by the Golgi. Scale bar, 10 μm. (G) Quantification of the area occupied by the Golgi, measured in Metamorph, for the indicated conditions. The data for Nde1/NdeL1 iKO –/+ Dox are duplicated from Figure 1G. The data represent the mean area for all measured Golgi + SEM. Data were combined from three replicates for each condition. Across all replicates, the following numbers of cells were analyzed: WT, 135; E47A, 205; E118A R129A, 164. Statistical significance relative to control cells (Nde1/NdeL1 iKO – Dox) was determined by two-tailed Mann–Whitney tests. ****$p \leq 0.0001$; n.s., $p > 0.05$.

beads overnight prior to elution and analysis by mass spectrometry (Supplemental Table S1).

To probe where within the cell the Nde1_SSSC–proteasome interaction occurs, we isolated the nuclei from interphase cells prior to immunoprecipitating Nde1. Although we detected Nde1 in both the nuclear and cytoplasmic samples, we only identified proteasome peptides in the cytoplasmic sample (Figure 3C and Supplemental Table S1). Similarly, from mitotic cells, we detected an interaction between Nde1_SSSC and the proteasome in the cytoplasmic, but not the chromatin-bound, fraction (Figure 3C and Supplemental Table S1). Therefore, the Nde1_SSSC–proteasome interaction is unlikely to be associated with the DNA.

Thus, these data identify a robust paralogue- and isoform-specific interaction between the recently evolved isoform of Nde1 and the 26S proteasome in human cells.

Multiple regions within the Nde1 C-terminus contribute to the 26S proteasome interaction

The isoform specificity of the Nde1-proteasome interaction suggests that the C-terminus of Nde1_SSSC mediates this interaction. In agreement with this, immunoprecipitation of C-terminally tagged Nde1_SSSC did not isolate the proteasome (Supplemental Table S1). In addition, a C-terminal truncation of Nde1, $Nde1^{1\text{-}265}$, failed to isolate the proteasome (Figure 4A and Supplemental Table S1). Because amino acid 316 is the C-terminal residue of the last shared exon between Nde1_SSSC and Nde1_KMLL, we expected that $Nde1^{1\text{-}316}$ would also fail to immunoprecipitate the proteasome. However, we found that $Nde1^{1\text{-}316}$ (Supplemental Table S1), as well as a further truncation to residue 283 (Figure 4A and Supplemental Table S1), both immunoprecipitated the proteasome. Thus, regions present within Nde1_KMLL

A

Bait:	GFP-Nde1_SSSC		GFP-Nde1_KMLL	GFP-NdeL1
	Asynchronous	Mitotic	Asynchronous	Mitotic
	# of peptides (% sequence coverage)			
GFP	1546 (88%)	300 (58%)	233 (61%)	713 (67%)
Nde1	990 (85%)*	354 (85%)*	200 (74%)*	81 (87%)*
NdeL1	19 (45%)*	17 (42%)*	2 (20%)*	443 (66%)*
Nde1/NdeL1	76	24	28	30
CENPF	14 (6%)	6 (3%)	-	26 (7%)
DYNC1H1	43 (11%)	2 (1%)	-	-
DYNC1I2	3 (9%)	-	-	-
DYNLL1	3 (27%)	-	-	-
DYNLL2	-	-	-	-
Lis1	129 (59%)	-	-	63 (49%)
DISC1	-	-	-	-
YWHAE	2 (18%)	2 (14%)	-	4 (26%)
26S Proteasome: PSMA1	19 (46%)	12 (26%)	-	-
PSMA2	12 (24%)	8 (30%)	-	-
PSMA3	6 (18%)	2 (9%)	-	-
PSMA4	11 (25%)	5 (14%)	-	-
PSMA5	10 (32%)	5 (22%)	2 (13%)	-
PSMA6	8 (24%)	12 (31%)	-	-
PSMA7	20 (46%)	15 (40%)	-	-
PSMB1	7 (33%)	6 (27%)	-	-
PSMB2	9 (36%)	5 (19%)	-	-
PSMB3	-	-	-	-
PSMB4	8 (31%)	4 (22%)	-	-
PSMB5	9 (27%)	4 (14%)	-	-
PSMB6	4 (25%)	5 (25%)	-	-
PSMB7	2 (9%)	-	-	-
PSMB9	2 (12%)	-	-	-
PSMC1	20 (39%)	10 (21%)	-	-
PSMC2	15 (35%)	10 (30%)	-	-
PSMC3	23 (45%)	19 (44%)	-	-
PSMC4	27 (53%)	19 (31%)	-	-
PSMC5	26 (40%)	17 (34%)	-	-
PSMC6	24 (39%)	25 (38%)	-	-
PSMD1	29 (27%)	9 (14%)	-	-
PSMD2	44 (37%)	15 (18%)	-	-
PSMD3	25 (37%)	12 (24%)	-	-
PSMD6	15 (29%)	4 (12%)	-	-
PSMD7	19 (44%)	9 (28%)	-	-
PSMD8	9 (28%)	-	-	-
PSMD11	22 (41%)	15 (30%)	-	-
PSMD12	19 (38%)	5 (14%)	-	-
PSMD14	15 (48%)	4 (23%)	-	-

C

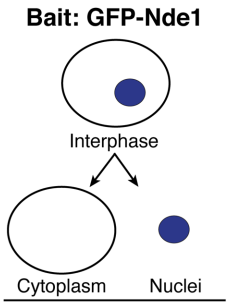

	Cytoplasm	Nuclei
GFP	291 (74%)	74 (53%)
Nde1	220 (80%)*	149 (79%)*
26S Proteasome	39 (5-26%) 12 subunits	0 subunits

D

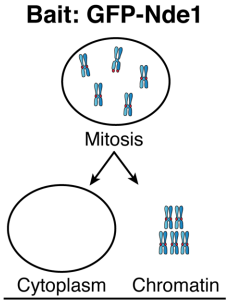

	Cytoplasm	Chromatin
GFP	238 (53%)	37 (36%)
Nde1	262 (78%)*	58 (72%)
26S Proteasome	306 (9-40%) 26 subunits	0 subunits

B

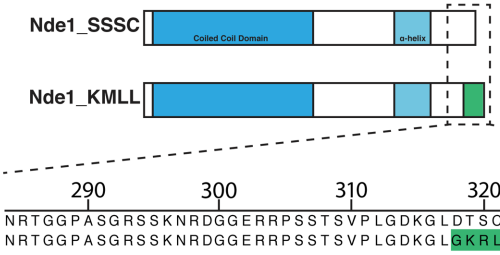

	GFP	Nde1	26S Proteasome
	# of peptides (% sequence coverage)		
Nde1_SSSC	652 (83%)	435 (77%)*	396 (9-50%) 28 subunits
Nde1_KMLL	449 (63%)	295 (77%)*	8 (4-11%) 3 subunits

FIGURE 3: Identification of a paralogue- and isoform-specific interaction between Nde1_SSSC and the 26S proteasome. (A) Summary of the mass spectrometry data for the immunoprecipitation of Nde1_SSSC, Nde1_KMLL, or NdeL1 from the indicated HeLa cell populations. Gene names are listed here. See Supplemental Table S1 for the corresponding protein names and a more complete listing of the identified proteins. The values represent the total number of peptides identified and the percent sequence coverage for the proteins encoded for by the indicated gene. For Nde1 and NdeL1, the asterisks indicate that the peptide count listed has been filtered to remove peptides assigned to both paralogues by SEQUEST due to the high sequence similarity. The percentage sequence coverage indicates the original SEQUEST determination. The numbers of identified peptides shared by both Nde1 and NdeL1 are listed as Nde1/NdeL1. (B) Schematic and sequence alignment of Nde1_SSSC and Nde1_KMLL, and summary of the mass spectrometry data for the immunoprecipitation of both isoforms from an asynchronous population of U2OS cells as in A. The region highlighted in green is the last exon of Nde1_KMLL and the only sequence differences distinguishing the two isoforms. (C) Summary of the mass spectrometry data for the immunoprecipitation of Nde1 from the cytoplasm or nuclei of asynchronous HeLa cells. The numbers of identified peptides and percentage sequence coverage are shown, as in A. For Nde1, the asterisks indicate that the peptide count listed has been filtered to remove peptides assigned to both Nde1 and NdeL1, as in A. For the 26S proteasome, the total number of peptides from all proteasomal subunits, the range of sequence coverages for the identified subunits, and the numbers of subunits identified are shown. Blue text indicates a detected proteasome interaction based off the presence of peptides from at least 12 proteasomal subunits. (D) Summary of the mass spectrometry data for the immunoprecipitation of Nde1 from the cytoplasmic or chromatin fractions of mitotic HeLa cells as in B.

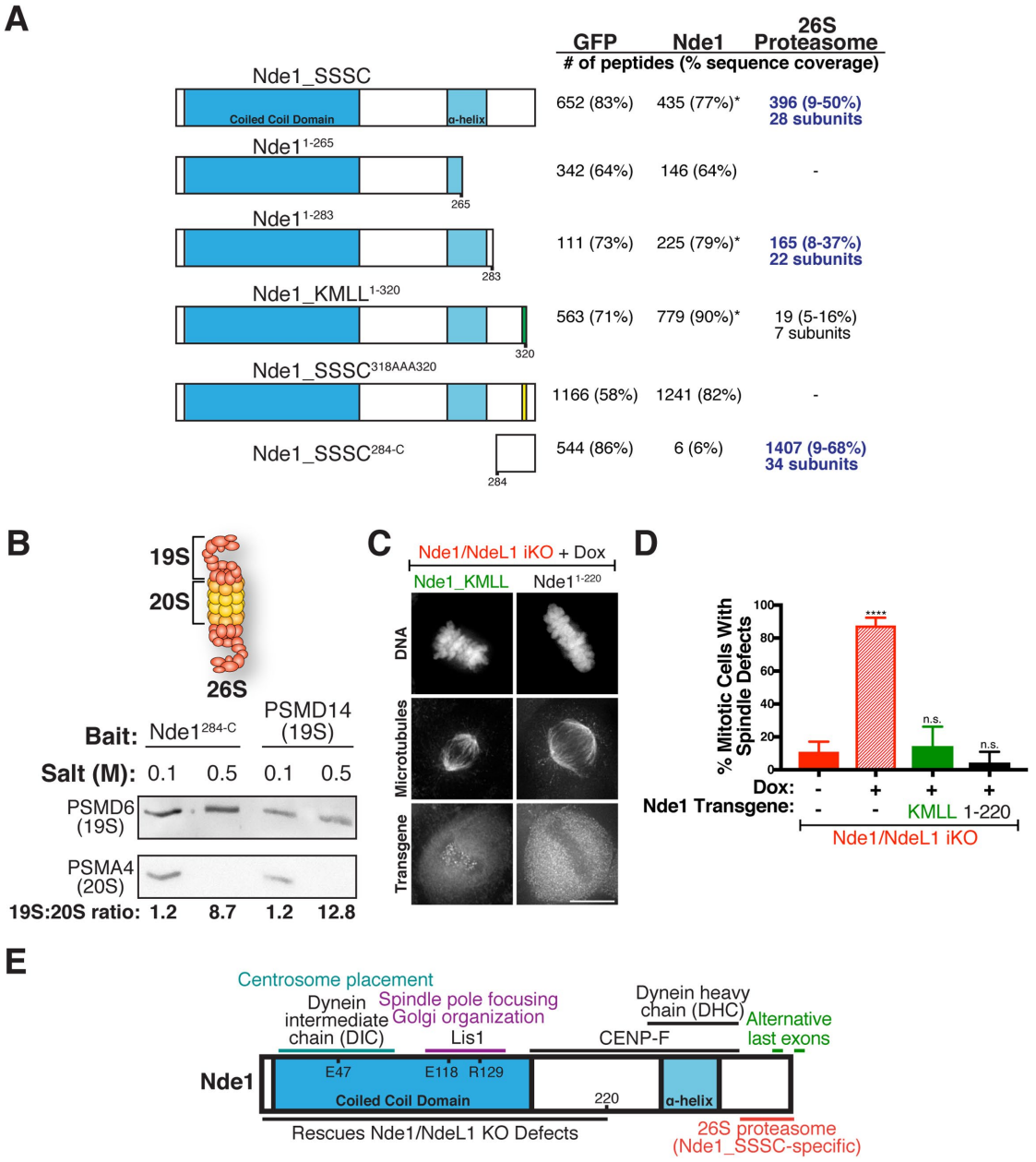

FIGURE 4: Identification of an isoform-specific proteasome interaction mediated by the 19S regulatory particle. (A) Summary of the mass spectrometry data for the immunoprecipitation of the indicated Nde1 truncations or fragments from asynchronous U2OS cells. The data for Nde1_SSSC are duplicated from Figure 3B. The numbers of identified peptides and percentage sequence coverage are shown. For Nde1, the asterisks indicate that the peptide count listed has been filtered to remove peptides assigned to both Nde1 and NdeL1. For the 26S proteasome, the total number of peptides from all proteasome subunits, the range of sequence coverages for the identified subunits, and the numbers of subunits identified are shown. Blue text indicates a detected proteasome interaction based off the presence of peptides from at least 12 proteasomal subunits. (B) Cartoon of the 26S proteasome and Western blots probing for a 19S subunit (PSMD6) and a 20S subunit (PSMA4) in the eluates of immunoprecipitations with the indicated buffer conditions. GFP-Nde1$^{284\text{-}C}$ or GFP-PSMD14 was expressed in U2OS cells and used as bait in the immunoprecipitations. The ratio of 19S to 20S was determined by quantifying the band intensities in Image Studio Lite. (C) Immunofluorescence images of DNA (Hoechst), microtubules (DM1A), and the indicated GFP-Nde1 variant 4 d after Cas9 induction with doxycycline. Scale bar, 10 µm. (D) Quantification of the spindle pole focusing defects for the indicated conditions. The data for Nde1/NdeL1 iKO –/+ Dox are duplicated from Figures 1C and 2C. The data represent the mean of three replicates + SD. Each replicate included ≥15 cells. Across all replicates, the following numbers of cells were analyzed: Nde1_KMLL, 70; Nde1$^{1\text{-}220}$, 59. Statistical significance relative to control cells (Nde1/NdeL1 iKO – Dox) was determined by two-tailed unpaired *t* tests. ****$p \leq 0.0001$; n.s., $p > 0.05$. (E) Updated schematic from Figure 2A indicating the interactions shown here to be required for spindle pole focusing, Golgi organization, and prophase centrosome placement, as well as the paralogue- and isoform-specific interaction between the C-terminus of Nde1_SSSC and the 26S proteasome. The binding region for CENP-F was determined in Soukoulis *et al.* (2005) and for DHC in Sasaki *et al.* (2000).

interact with the proteasome, even though full-length Nde1_KMLL does not. We therefore sought to test whether the Nde1_KMLL C-terminus inhibits the interaction with the proteasome. Remarkably, we found that Nde1_KMLL$^{1\text{-}320}$, which has only three isoform-specific residues (amino acids 318–320—the first residue encoded by the isoform-specific exons is identical; Figure 3B), is defective in proteasome binding (Figure 4A and Supplemental Table S1). We also tested the contribution of the C-terminus of Nde1_SSSC to the proteasome interaction and found that mutating residues 318–320 of the canonical Nde1 isoform to alanine (Nde1^{318AAA320}) prevented the interaction with the proteasome (Figure 4A and Supplemental Table S1). The isoform specificity of the Nde1 interaction with the 26S proteasome is therefore established not only by residues in Nde1_KMLL that prevent binding to the proteasome but also by residues specific to Nde1_SSSC that positively contribute to proteasome binding.

To identify a region of Nde1 that was sufficient to interact with the proteasome, we next tested Nde1 C-terminal fragments. In agreement with our finding that Nde1$^{1\text{-}265}$ does not immunoprecipitate the proteasome, we detected an interaction between Nde1_SSSC$^{266\text{-}C}$ and the proteasome (Supplemental Table S1), indicating that the Nde1_SSSC C-terminus is both necessary and sufficient for the interaction with the 26S proteasome. Additionally, a more minimal C-terminal fragment, Nde1_SSSC$^{284\text{-}C}$, also immunoprecipitated the proteasome (Figure 4A and Supplemental Table S1). Because both Nde1$^{1\text{-}283}$ and Nde1_SSSC$^{284\text{-}C}$ are able to immunoprecipitate the proteasome, we conclude that multiple regions C-terminal to residue 265 in the canonical human isoform contribute to the 26S proteasome interaction.

Nde1 associates with the 19S regulatory particle

The 26S proteasome is a macromolecular complex responsible for the majority of the regulated protein degradation in eukaryotic cells (Glickman and Ciechanover, 2002). In immunoprecipitations using a tagged proteasome subunit, we did not identify Nde1 peptides (Supplemental Table S1), suggesting that Nde1 likely associates with only a subset of the total cellular proteasome population. However, as the proteasome is highly abundant in eukaryotic cells (Tanaka *et al.*, 1986), even a small Nde1-bound proteasome population could have significant cellular consequences.

Two subcomplexes—a 20S core particle containing the degradative subunits and a 19S regulatory complex—form the 26S proteasome (Figure 4B) (Kish-Trier and Hill, 2013). To determine which proteasome subcomplex associates with Nde1, we took advantage of the inherent salt sensitivity of the 26S holocomplex in vitro (Verma *et al.*, 2000). When purified in a buffer containing a low concentration of salt and supplemented ATP, the entire 26S proteasome can be purified from human cells (Figure 4B, Supplemental Figure S3A, and Supplemental Table S1). However, at increased salt concentrations, the 26S proteasome dissociates into its two constituent subcomplexes, resulting in purifications enriched for the subcomplex containing the tagged subunit (Figure 4B and Supplemental Figure S3A). Consistent with an interaction with the 26S proteasome, immunoprecipitation of Nde1 under low salt conditions isolated representative subunits of both the 19S and 20S (Figure 4B and Supplemental Figure S3B). However, at higher salt concentrations, the 19S proteasome was enriched (Figure 4B and Supplemental Figure S3B), suggesting that the primary Nde1-proteasome interaction site likely exists within the 19S regulatory particle.

Together, these data define the molecular basis for an interaction between the recently evolved human Nde1 isoform and the 19S regulatory particle of the 26S proteasome.

The Nde1–proteasome interaction is not required for core cellular roles of dynein

Having identified a robust association between Nde1 and the proteasome, we sought to test the functional contribution of this interaction. The minimal region of Nde1 that is sufficient for immunoprecipitating the proteasome (Nde1_SSSC$^{284\text{-}C}$) is C-terminal to any region previously implicated in dynein binding or regulation, suggesting that the Nde1-proteasome interaction is unlikely to be required for the core cellular roles of dynein. Indeed, expression of the alternative human isoform, Nde1_KMLL, which does not interact with the proteasome, rescued the spindle pole focusing (Figure 4, C and D) and centrosome placement (Supplemental Figure S4A) defects in the Nde1/NdeL1 double knockout cells. We also found that an Nde1$^{1\text{-}220}$ truncation, which lacks the Nde1_SSSC C-terminus, rescues the Nde1/NdeL1 double knockout defects in spindle pole focusing (Figure 4, C and D) and Golgi organization (Supplemental Figure S4B).

Loss of Nde1 alone from human cells in culture does not result in severe phenotypic consequences (McKinley and Cheeseman, 2017). However, Nde1 is essential for neurodevelopment. Therefore, although likely dispensable for cell viability in culture, the Nde1-proteasome interaction may be required specifically during development of the human brain. Because of the diverse cellular roles of Nde1, testing the functional consequence of the Nde1-proteasome interaction will require Nde1 mutants that specifically disrupt the proteasome interaction without altering other Nde1 functions. To date, the C-terminal exons of Nde1 do not have other ascribed functions (Mosca *et al.*, 2017). Thus, the C-terminal mutations we identify here that prevent the interaction with the proteasome will facilitate future work investigating the contribution of the Nde1-proteasome interaction in human neurodevelopment.

DISCUSSION

As a key regulator of cytoplasmic dynein, Nde1 contributes to diverse cellular processes. Prior work has suggested that dynein regulation is achieved through the coordinated functions of Nde1 and Lis1, with Nde1 acting to help recruit Lis1 to dynein (McKenney *et al.*, 2010; Wang and Zheng, 2011; Huang *et al.*, 2012). Our dissection of the molecular features of Nde1 required for diverse functions of dynein indicates that the role of Nde1 in dynein regulation is more complex than previously appreciated. A direct Nde1–Lis1 interaction is required for spindle pole focusing (Figures 2, B and C, and 4E) and Golgi organization (Figures 2, F and G, and 4E), but it is largely dispensable for positioning the centrosomes during prophase (Figures 2, D and E, and 4E), even though Lis1 itself is required (Figure 1E and Supplemental Figure S1B). Thus, the contribution of Nde1 to dynein regulation is not limited to solely helping recruit Lis1 to dynein. Additionally, our work indicates that dynein regulation is accomplished not only through the presence or absence of specific adaptor proteins but also through changes in the intermolecular interactions within those adaptor proteins. These altered interactions may allow for precise adjustments of dynein activity to optimize the force output required in each cellular context.

Our work also indicates that the cellular functions of Nde1 include not only dynein regulation, but also a 26S proteasome interaction (Figures 3A and 4E). Intriguingly, although the Nde1_KMLL isoform is widely conserved among mammals, the proteasome-binding isoform, Nde1_SSSC, only has homologues in a small subset of mammals and is absent from mice. A potential role for the Nde1–proteasome interaction in brain development could contribute to the increased phenotypic severity of human Nde1 mutations as compared with mouse Nde1 knockouts (Bakircioglu *et al.*, 2011). Additionally, a dual role of Nde1 in both interacting with the

proteasome and regulating dynein could explain why the loss of many other dynein-interacting or centrosomal proteins results in less-severe brain phenotypes than those resulting from loss of Nde1 (Doobin *et al.*, 2016). An Nde1–proteasome interaction, either in conjunction with or independent of dynein, could also contribute to normal brain development. For example, during neuronal maturation, an asymmetric distribution of proteasomes within axons, created by dynein-mediated transport, is required for proper axonal growth (Hsu *et al.*, 2015). Thus, identifying the function of the interaction between Nde1 and the 26S proteasome has potentially significant implications for understanding human neurodevelopment in physiological and disease states. However, analyzing the functional contribution of the Nde1–proteasome interaction to brain development also represents a significant challenge since the interaction is specific to the human Nde1 isoform and therefore cannot be studied in mouse models. Future work using three-dimensional cerebral organoid culture systems and the precise Nde1 mutants we have identified here that are defective in associating with the proteasome will facilitate identification of the role of the Nde1–proteasome interaction in human neurodevelopment.

MATERIALS AND METHODS

Molecular biology

The sgRNA targeting dynein intermediate chain (DYNC1I2: 5′ attactgtacctagatccca 3′) was cloned into pLenti-sgRNA. Except for Nde1_KMLL, all GFP-tagged constructs for expression in human cells were generated by cloning the cDNA into a pBABEblast vector containing either an N-terminal LAP tag (GFP-TEV-S) or a C-terminal LAP tag (His-PreScission-GFP) as described previously (Cheeseman and Desai, 2005). Nde1_KMLL was generated by two rounds of overlap extension PCR from the Nde1_SSSC cDNA followed by cloning into the N-terminal LAP tag pBABEblast vector. The Nde1_KMLL-specific sequence was codon optimized for expression in human cells. Mutations in Nde1 were introduced by site-directed mutagenesis. An *Escherichia coli* codon optimized version of Nde1 was expressed in cells requiring a CRISPR/Cas9 resistant transgene. In all cases, the inserted cDNA was verified by sequencing. Plasmids will be deposited to Addgene.

Cell culture and cell line generation

All HeLa (female cervix adenocarcinoma cells, not authenticated) and U2OS (female osteosarcoma cells, not authenticated) used in this study were cultured in DMEM supplemented with 10% fetal bovine serum (FBS; GE Healthcare), 100 U/ml penicillin, 100 U/ml streptomycin, and 2 mM L-glutamine at 37°C with 5% CO_2. Inducible knockout lines were cultured in media containing certified tetracycline-free FBS (Gemini Bio-Products). Cell lines were tested for mycoplasma contamination monthly.

The Nde1/NdeL1, dynein heavy chain, and Lis1 CRISPR/Cas9-based inducible knockout cell lines were described in McKinley and Cheeseman (2017) and the dynein intermediate chain inducible knockout cell line was generated by the same protocol of lentiviral transduction of the sgRNA containing vector into HeLa cells containing Cas9 under the control of a doxycycline-inducible promoter. Cells expressing guide resistant GFP-Nde1 constructs were generated by retroviral infection of the Nde1/NdeL1 inducible knockout cell line followed by blasticidin selection. These blasticidin-resistant polyclonal cell lines were used for all analyses to minimize potential variation in the efficiency of CRISPR/Cas9 induction and cutting between different replacement cell lines. For the Nde1$^{1\text{-}220}$ replacement cell line, the transgene expression levels were low, even after selection, so flow cytometry was performed to generate a population of cells that were enriched for transgene expression. To induce Cas9 expression, cells were dosed with 1 µg/ml doxycycline at 0, 24, and 48 h and assayed at 96 h (4 d).

Cell lines expressing GFP-tagged constructs for immunoprecipitation and mass spectrometry analysis were generated by retroviral infection of either HeLa or U2OS cells followed by single cell sorting.

Immunofluorescence

Cells were plated on glass coverslips coated with poly-L-lysine (Sigma-Aldrich). For all experiments except where Golgi staining was performed, cells were fixed with 4% formaldehyde in PHEM buffer (60 mM PIPES, 25 mM HEPES, 10 mM ethylene glycol tetraacetic acid [EGTA], and 4 mM $MgSO_4$, pH 7) for 10 min. Blocking and all antibody dilutions were performed using AbDil (20 mM Tris, 150 mM NaCl, 0.1% Triton X-100, 3% bovine serum albumin [BSA], and 0.1% NaN_3, pH 7.5). Phosphate-buffered saline (PBS) plus 0.1% Triton X-100 (PBS-TX) was used for washes. For Golgi staining, cells were fixed with 4% formaldehyde in PBS for 15 min. Blocking and all antibody dilutions were performed using PBS plus 1% BSA and 0.3% Triton X-100. Anti-GM130 antibody (Cell Signaling Technologies) was used at a 1:3200 dilution. PBS was used for washes. For all experiments, GFP-Booster (Chromotek; 1:200 dilution) was used to amplify the fluorescence of the GFP-tagged transgenes and DM1A was used to stain the microtubules (Sigma-Aldrich; 1:3000 dilution). Anti-mouse Cy3-conjugated secondary antibody (Jackson ImmunoResearch Laboratories) was used at 1:300. DNA was visualized by incubating cells in 1 µg/ml Hoechst-33342 (Sigma-Aldrich) in PBS-TX for 10 min. Coverslips were mounted using 0.5% *p*-phenylenediamine and 20 mM Tris-Cl, pH 8.8, in 90% glycerol.

Fluorescence microscopy

Images were acquired on a DeltaVision Core microscope (Applied Precision) equipped with a CoolSnap HQ2 CCD camera (Photometrics) and a 100×, 1.4-NA U-PlanApo objective (Olympus). Images displayed in the figures were deconvolved and maximally projected. The fluorescence is not scaled equivalently in each panel due to image acquisition on different days.

For the blasticidin-resistant cell lines expressing GFP-Nde1 variants, only GFP-positive cells were analyzed. "GFP positive" was defined as having cytoplasmic fluorescence ≥2.5 times above the background signal in a nonfluorescent cell.

Mitotic spindle pole focusing was analyzed by examining 100 cells for each condition (one replicate) and denoting the percentage of cells with defects in bipolar spindle assembly. Three to five biological replicates were analyzed for each condition, and the mean percentage of cells (+SD) with abnormal spindles for those replicates was plotted.

Prophase cells analyzed for proper centrosome placement were found by the presence of condensed DNA, foci of microtubule nucleation visualized by DM1A staining, and the inference of a nuclear envelope by DM1A exclusion from the DNA mass. Only cells with exactly two foci of microtubule nucleation were analyzed. Five *Z*-sections with 1-µm spacing were acquired for each cell. The distance between the center of the microtubule nucleation foci and the closest point of in-focus DNA was determined for each centrosome using the DeltaVision software. The mean (+SEM) of all measured centrosome-nucleus distances for each condition was plotted.

For analysis of the Golgi organization, five *Z*-sections with 1-µm spacing were acquired for each cell. Images were maximally projected and analyzed in Metamorph (Molecular Devices) by drawing the minimal region encompassing the Golgi and denoting the

region area for each cell. The mean (+SEM) of all measured Golgi occupancy areas for each condition was plotted.

In all cases, sample sizes were chosen to capture a diversity of cells. Because of the nature of the inducible knockout system and our population level analyses, we note that not every cell analyzed is fully depleted for the targeted gene. For this reason, Mann–Whitney tests were used to analyze the centrosome–nuclei distance and Golgi area data. This incomplete penetrance results in our reported mean centrosome–nuclei distances and Golgi areas for the knockout conditions underestimating the severity of the observed defects in individual knockout cells.

Immunoprecipitations

For mitotic immunoprecipitations, cells from 60x 15-cm plates were arrested with 330 nM nocodazole (Sigma-Aldrich) for 14 h and harvested by shake-off. The cells remaining on the plates following the mitotic shake-off were collected for interphase samples. Asynchronous populations were obtained by harvesting all of the cells from 30x 15-cm plates.

Nde1 and NdeL1 immunoprecipitations for mass spectrometry analysis were performed as described previously (Cheeseman and Desai, 2005). Briefly, harvested cells were washed in PBS and resuspended 1:1 in 50 mM HEPES, 1 mM EGTA, 1 mM $MgCl_2$, 100 mM KCl, 10% glycerol, pH 7.4 (1X lysis buffer), before freezing in liquid nitrogen. To thaw, an equal volume of 1.5× lysis buffer supplemented with 0.075% Nonidet P-40 (NP-40) was added to the resuspended cells. Complete EDTA-free protease inhibitor cocktail (Roche) and 1 mM phenylmethylsulfonyl fluoride (PMSF) was added to inhibit proteases. Beta-glycerophosphate (20 mM) and 0.4 mM sodium orthovanadate were added to inhibit phosphatases. Cells were lysed by sonication, and the lysate was cleared by centrifugation. The cleared supernatant was mixed with Protein A beads (Bio-Rad) coupled to GFP antibody (Cheeseman and Desai, 2005). Potassium chloride was supplemented to a final concentration of 300 mM, and the sample was placed on a rotating wheel for 1 h at 4°C. The beads were washed five times in 50 mM HEPES, 1 mM EGTA, 1 mM $MgCl_2$, 300 mM KCl, 10% glycerol, 0.05% NP-40, 1 mM dithiothreitol (DTT), 10 µg/ml leupeptin, 10 µg/ml pepstatin, 10 µg/ml chymostatin, pH 7.4 (wash buffer), and once in wash buffer without detergent. Protein was eluted with 0.1 M glycine, pH 2.6. The eluate was precipitated with trichloroacetic acid (TCA) and digested with Lys-C (Sigma-Aldrich) and trypsin (Promega) for analysis by mass spectrometry.

For isolation of nuclei or chromatin from interphase or mitotic cells, respectively, frozen cells were resuspended in 300 mM sucrose, 50 mM Tris, 25 mM KCl, 5 mM $MgCl_2$, pH 7.5 (sucrose homogenization buffer), supplemented with Complete EDTA-free protease inhibitor cocktail, 1 mM PMSF, 20 mM beta-glycerophosphate, and 0.4 mM sodium orthovanadate. Additional 2 M sucrose was added to bring the final sucrose concentration to 300 mM. Thawed cells were dounce homogenized on ice with 15–25 strokes over 5 min. Lysed cells were spun at 5000 rpm for 8 min. The supernatant was removed and saved as the cytoplasmic fraction. The pellet was resuspended in sucrose homogenization buffer and used as the nuclear/chromatin-bound fractions. All samples were then sonicated and spun at 20,000 rpm for 10 min. The resulting supernatants were incubated with Protein A beads (Bio-Rad) coupled to GFP antibody (Cheeseman and Desai, 2005), and the rest of the immunoprecipitation was carried out as for Nde1 above.

The proteasome immunoprecipitations in Supplemental Figure S3A were performed with the protocol above except the protein was eluted by incubating the beads in a buffer containing PreScission (HRV 3C) protease at 4°C overnight. The eluted protein was then analyzed by SDS–PAGE and stained with Coomassie. The low-salt PMSD14 IP in Supplemental Figure S3 and Supplemental Table S1 had the following additional changes: 50 µg/ml creatine kinase (Roche), 35 mM creatine phosphate (Roche), and 5 mM ATP (ATP regeneration system) were added to the thawed cells and again to the cleared supernatant, no additional KCl was added to the cleared supernatant, and 2 mM ATP was added to the wash buffers. For mass spectrometry analysis, a portion of the eluted protein was TCA precipitated and then digested with the standard protocol.

For the Nde1 and proteasome immunoprecipitations analyzed by Western blotting in Figure 4B and Supplemental Figure S3B, the cell pellets were resuspended in 1x lysis buffer plus 1% Triton X-100 and split into two samples, with ATP regeneration system added to one of the samples for each cell line. The cells were allowed to lyse on ice for 30 min with occasional vortexing, then spun at 16,000 rpm for 10 min. The resulting supernatants were mixed with Protein A beads (Bio-Rad) coupled to GFP antibody (Cheeseman and Desai, 2005), supplemented with either ATP regeneration system or KCl to adjust the salt concentration to 300 mM or 500 mM, and incubated at 4°C for 1 h. The beads were washed six times with wash buffer supplemented with either 2 mM ATP or KCl to adjust the salt concentration to 300 mM or 500 mM. Glycine elutions and TCA precipitations were performed as described above followed by Western blot analysis.

Mass spectrometry

Immunoprecipitated proteins were analyzed on an LTQ XL Ion trap mass spectrometer (ThermoFisher Scientific), and the data were analyzed using SEQUEST software as described previously (Washburn *et al.*, 2001). The percentage sequence coverage indicated in the figures is for the isoform identified by SEQUEST and should be taken as an approximation.

Western blotting

For Western blotting, samples were separated on a 12% SDS–PAGE gel, semidry transferred to nitrocellulose and blocked for 1 h in 3% BSA in TBS + 0.1% Tween-20 (blocking buffer). Primary antibodies (Anti-PSMD6/Rpn7 and Anti-PSMA4/a3 [Enzo Life Sciences]) were diluted 1:1000 in blocking buffer. HRP-conjugated secondary antibodies (Kindle Biosciences) were used at 1:1000 and diluted in TBS + 0.1% Tween-20. All antibody incubations were performed at room temperature for 1 h. Washes were performed with TBS + 0.1% Tween-20. Clarity (Bio-Rad) was used as the enhanced chemiluminescence (ECL) substrate. Images were acquired with a KwikQuant Imager (Kindle Biosciences) and converted to black and white using the blue filter in Adobe Photoshop. Band intensities were quantified in Image Studio Lite using grayscale images.

ACKNOWLEDGMENTS

We thank the members of the Cheeseman lab and Sara Dubbury for discussions and input on the article. This work was supported by grants from The Harold G. and Leila Y. Mathers Charitable Foundation and the National Institutes of Health/National Institute of General Medical Sciences (GM088313 and GM108718) to I.M.C. and a National Science Foundation Graduate Research Fellowship under Grant No. 1122374 to J.K.M.

REFERENCES

Alkuraya FS, Cai X, Emery C, Mochida GH, Al-Dosari MS, Felie JM, Hill RS, Barry BJ, Partlow JN, Gascon GG, *et al.* (2011). Human mutations in NDE1 cause extreme microcephaly with lissencephaly [corrected]. Am J Hum Genet 88, 536–547.

Bakircioglu M, Carvalho OP, Khurshid M, Cox JJ, Tuysuz B, Barak T, Yilmaz S, Caglayan O, Dincer A, Nicholas AK, *et al.* (2011). The essential role of centrosomal NDE1 in human cerebral cortex neurogenesis. Am J Hum Genet 88, 523–535.

Bolhy S, Bouhlel I, Dultz E, Nayak T, Zuccolo M, Gatti X, Vallee R, Ellenberg J, Doye V (2011). A Nup133-dependent NPC-anchored network tethers centrosomes to the nuclear envelope in prophase. J Cell Biol 192, 855–871.

Bradshaw NJ, Christie S, Soares DC, Carlyle BC, Porteous DJ, Millar JK (2009). NDE1 and NDEL1: multimerisation, alternate splicing and DISC1 interaction. Neurosci Lett 449, 228–233.

Bradshaw NJ, Hayashi MA (2017). NDE1 and NDEL1 from genes to (mal) functions: parallel but distinct roles impacting on neurodevelopmental disorders and psychiatric illness. Cell Mol Life Sci 74, 1191–1210.

Bradshaw NJ, Hennah W, Soares DC (2013). NDE1 and NDEL1: twin neurodevelopmental proteins with similar "nature" but different "nurture." Biomol Concepts 4, 447–464.

Cheeseman IM, Desai A (2005). A combined approach for the localization and tandem affinity purification of protein complexes from metazoans. Sci STKE 2005, pl1.

Derewenda U, Tarricone C, Choi WC, Cooper DR, Lukasik S, Perrina F, Tripathy A, Kim MH, Cafiso DS, Musacchio A, *et al.* (2007). The structure of the coiled-coil domain of Ndel1 and the basis of its interaction with Lis1, the causal protein of Miller-Dieker lissencephaly. Structure 15, 1467–1481.

Dobyns WB, Das S (2009). LIS1-associated lissencephaly/subcortical band heterotopia. In: GeneReviews® [Internet], ed., MP Adam, HH Ardinger, RA Pagon, *et al.*, Seattle: University of Washington, 1993–2018. Available from www.ncbi.nlm.nih.gov/books/NBK5189/.

Doobin DJ, Kemal S, Dantas TJ, Vallee RB (2016). Severe NDE1-mediated microcephaly results from neural progenitor cell cycle arrests at multiple specific stages. Nat Commun 7, 12551.

Glickman MH, Ciechanover A (2002). The ubiquitin-proteasome proteolytic pathway: destruction for the sake of construction. Physiol Rev 82, 373–428.

Guven A, Gunduz A, Bozoglu TM, Yalcinkaya C, Tolun A (2012). Novel NDE1 homozygous mutation resulting in microhydranencephaly and not microlyssencephaly. Neurogenetics 13, 189–194.

Hsu MT, Guo CL, Liou AY, Chang TY, Ng MC, Florea BI, Overkleeft HS, Wu YL, Liao JC, Cheng PL (2015). Stage-dependent axon transport of proteasomes contributes to axon development. Dev Cell 35, 418–431.

Huang J, Roberts AJ, Leschziner AE, Reck-Peterson SL (2012). Lis1 acts as a "clutch" between the ATPase and microtubule-binding domains of the dynein motor. Cell 150, 975–986.

Kardon JR, Vale RD (2009). Regulators of the cytoplasmic dynein motor. Nat Rev Mol Cell Biol 10, 854–865.

Kish-Trier E, Hill CP (2013). Structural biology of the proteasome. Annu Rev Biophys 42, 29–49.

Lam C, Vergnolle MA, Thorpe L, Woodman PG, Allan VJ (2010). Functional interplay between LIS1, NDE1 and NDEL1 in dynein-dependent organelle positioning. J Cell Sci 123, 202–212.

McKenney RJ, Vershinin M, Kunwar A, Vallee RB, Gross SP (2010). LIS1 and NudE induce a persistent dynein force-producing state. Cell 141, 304–314.

McKinley KL, Cheeseman IM (2017). Large-scale analysis of CRISPR/Cas9 cell-cycle knockouts reveals the diversity of p53-dependent responses to cell-cycle defects. Dev Cell 40, 405–420 e402.

Mosca S, Raponi M, Meneghello A, Buratti E, Woods CG, Baralle D (2017). Human NDE1 splicing and mammalian brain development. Sci Rep 7, 43504.

Paciorkowski AR, Keppler-Noreuil K, Robinson L, Sullivan C, Sajan S, Christian SL, Bukshpun P, Gabriel SB, Gleeson JG, Sherr EH, *et al.* (2013). Deletion 16p13.11 uncovers NDE1 mutations on the non-deleted homolog and extends the spectrum of severe microcephaly to include fetal brain disruption. Am J Med Genet Part A 161A, 1523–1530.

Raaijmakers JA, Tanenbaum ME, Medema RH (2013). Systematic dissection of dynein regulators in mitosis. J Cell Biol 201, 201–215.

Sasaki S, Shionoya A, Ishida M, Gambello MJ, Yingling J, Wynshaw-Boris A, Hirotsune S (2000). A LIS1/NUDEL/cytoplasmic dynein heavy chain complex in the developing and adult nervous system. Neuron 28, 681–696.

Soares DC, Bradshaw NJ, Zou J, Kennaway CK, Hamilton RS, Chen ZA, Wear MA, Blackburn EA, Bramham J, Bottcher B, *et al.* (2012). The mitosis and neurodevelopment proteins NDE1 and NDEL1 form dimers, tetramers, and polymers with a folded back structure in solution. J Biol Chem 287, 32381–32393.

Soukoulis V, Reddy S, Pooley RD, Feng Y, Walsh CA, Bader DM (2005). Cytoplasmic LEK1 is a regulator of microtubule function through its interaction with the LIS1 pathway. Proc Natl Acad Sci USA 102, 8549–8554.

Tan L, Bi B, Zhao P, Cai X, Wan C, Shao J, He X (2017). Severe congenital microcephaly with 16p13.11 microdeletion combined with NDE1 mutation, a case report and literature review. BMC Med Genet 18, 141.

Tanaka K, Ii K, Ichihara A, Waxman L, Goldberg AL (1986). A high molecular weight protease in the cytosol of rat liver. I. Purification, enzymological properties, and tissue distribution. J Biol Chem 261, 15197–15203.

Tarricone C, Perrina F, Monzani S, Massimiliano L, Kim MH, Derewenda ZS, Knapp S, Tsai LH, Musacchio A (2004). Coupling PAF signaling to dynein regulation: structure of LIS1 in complex with PAF-acetylhydrolase. Neuron 44, 809–821.

Verma R, Chen S, Feldman R, Schieltz D, Yates J, Dohmen J, Deshaies RJ (2000). Proteasomal proteomics: identification of nucleotide-sensitive proteasome-interacting proteins by mass spectrometric analysis of affinity-purified proteasomes. Mol Biol Cell 11, 3425–3439.

Wang S, Ketcham SA, Schon A, Goodman B, Wang Y, Yates J 3rd, Freire E, Schroer TA, Zheng Y (2013). Nudel/NudE and Lis1 promote dynein and dynactin interaction in the context of spindle morphogenesis. Mol Biol Cell 24, 3522–3533.

Wang S, Zheng Y (2011). Identification of a novel dynein binding domain in nudel essential for spindle pole organization in Xenopus egg extract. J Biol Chem 286, 587–593.

Washburn MP, Wolters D, Yates JR 3rd (2001). Large-scale analysis of the yeast proteome by multidimensional protein identification technology. Nat Biotechnol 19, 242–247.

Yan X, Li F, Liang Y, Shen Y, Zhao X, Huang Q, Zhu X (2003). Human Nudel and NudE as regulators of cytoplasmic dynein in poleward protein transport along the mitotic spindle. Mol Cell Biol 23, 1239–1250.

Zylkiewicz E, Kijanska M, Choi WC, Derewenda U, Derewenda ZS, Stukenberg PT (2011). The N-terminal coiled-coil of Ndel1 is a regulated scaffold that recruits LIS1 to dynein. J Cell Biol 192, 433–445.